IDE**A**L®

Kinetics of the Formation and Dissolution of Ni Precipitates in a Gibbsite/Amorphous Silica Mixture

Kirk G. Scheckel[1] and Donald L. Sparks

Department of Plant and Soil Sciences, University of Delaware, 147 Townsend Hall, Newark, Delaware 19717-1303

There have been a number of studies that have examined metal precipitation reactions on an array of natural soil materials. While many of these investigations have focused on model single-component systems, recent research has appeared on metal precipitation on soils and clay fractions of soils. However, few studies have explored mixed model component systems, which may lead to a better understanding of metal reactions on soils and clay fractions. Furthermore, only a few studies have appeared on the stability of the metal surface precipitates. In light of this, we investigated Ni sorption and dissolution kinetics and mechanisms on a mixture of gibbsite and amorphous silica by combining macroscopic studies with X-ray absorption fine structure (XAFS) and diffuse reflectance spectroscopies (DRS), and high-resolution thermogravimetric analysis (HRTGA). Batch sorption experiments were conducted at pH 7.5 and at different reaction times to elucidate the sorption process and to study the role of residence time on metal precipitate stability. Spectroscopic and HRTGA investigations revealed α-Ni(OH)$_2$ precipitates formed on the gibbsite/silica mixture initially and over time evolved to a Ni phyllosilicate. The available Si source was derived from partial dissolution of the sorbent during Ni sorption. With increasing residence time, the precipitate phases drastically increased in stability, as shown by decreasing amounts of Ni release as effected by nitric acid (HNO$_3$) and ethylenediaminetetraacetic acid (EDTA) treatments. This aging effect may be explained by the silicate-for-nitrate exchange during the first days of reaction and subsequently by silicate polymerization and partial grafting onto the hydroxide layers to form a phyllosilicate precursor phase (R. G. Ford, A. C. Scheinost, K. G. Scheckel, and D. L. Sparks, *Environ. Sci. Technol.* 33(18), 3140–3144, 1999). © 2000 Academic Press

Key Words: metal precipitate formation and dissolution; sorption kinetics; XAFS; DRS; HRTGA; sorption in sorbent mixtures; residence (aging) time.

1. INTRODUCTION

Sorption reactions at the mineral/water interface largely determine the mobility and bioavailability of metals in soils and sediments. Spectroscopic and microscopic studies in the last decade showed the importance of metal hydroxide precipitate formation upon reacting a variety of model component clay mineral and ox-

ide surfaces with metals such as Ni or Co (2–4). In the case where the sorbent phase contained Al, the precipitates were predominantly Al-containing layered double-hydroxide (LDH) phases (2–9). In the case of Al-free sorbents, however, metal sorption resulted in α-type metal hydroxide precipitates (10, 9, 11).

Elzinga and Sparks (12) examined Ni sorption mechanisms in a 1 : 1 pyrophyllite–montmorillonite mixture at pH 7.5 and a reaction time of 40 min. XAFS was employed to estimate the distribution of Ni over the mixture components. The main modes of Ni uptake under these reaction conditions were adsorption on montmorillonite and surface precipitation on pyrophyllite. Batch sorption studies suggested that pyrophyllite sorbed slightly more Ni than montmorillonite. The results of this study indicate that both adsorption and surface precipitation are important mechanisms in the overall uptake of Ni by the clay mixture during the 40-min reaction period.

Roberts *et al.* (13) observed the formation of mixed Ni–Al LDH precipitates on the Ap horizon of Matapeake silt loam soil (Typic Hapludult) and its clay fraction over a pH range of 6.0–7.5. This was the first paper to extend the study of metal precipitation reactions from model component systems to a complex soil environment that contained an array of inorganic and organic components. XAFS analysis for the whole soil indicated a mixed Ni–Al phase formed at pH 7.5 after 24 h of reaction. XAFS investigations also detected the formation of Ni–Al LDH precipitates on the clay fraction of the soil within 15 min at pH 7.5 and 2 h at pH 6.8. Precipitates were not observed at pH 6.0 on the clay fraction, suggesting only adsorption phenomena were occurring.

Formation of metal precipitate phases drastically reduces metal concentrations in soil and sediment solutions and effectively competes with adsorption onto soil minerals (12). However, only a few investigations have assessed the stability of the surface precipitates. Scheidegger and Sparks (2) examined the dissolution of Ni–Al LDH precipitates formed on pyrophyllite using HNO$_3$ at pH 4 and 6. Nickel detachment was initially rapid at both pH values (with <10% of total Ni released), which was attributable to desorption of specifically adsorbed, mononuclear Ni. Dissolution then slowed, which was ascribed to the gradual dissolution of the precipitates. In comparison with a β-Ni(OH)$_2$ reference compound, the Ni–Al LDH surface precipitates were much more stable. Ford *et al.* (1) investigated the dissolution of

Ⓐ P

Ni–Al LDH surface precipitates on pyrophyllite using an EDTA solution at pH 7.5. Detachable Ni drastically decreased when the age of the precipitate increased from 1 h to 1 year. By employing HRTGA, which is sensitive to changes in the interlayer composition of the LDH, and by comparing the results for Ni sorption on pyrophyllite at different aging times with those of various reference compounds, Ford *et al.* (1) showed that a substantial part of the aging effect was due to replacement of interlayer nitrate by silicate, which transformed the initial Ni–Al LDH into a Ni–Al phyllosilicate precursor. The source of the silicate was the dissolving surface of the pyrophyllite. Scheckel *et al.* (14) investigated the dissolution of Ni–Al LDH phases on pyrophyllite and gibbsite and α-Ni(OH)$_2$ precipitates on talc employing EDTA (pH 7.5) and nitric acid (pH 4.0) for sorption aging times ranging from 1 h to 1 year. Using an array of analytical techniques, differences in stability of the surface precipitates could be explained by a combination of Al-for-Ni substitution in the hydroxide layers (for pyrophyllite and gibbsite) and silicate-for-nitrate substitution in the interlayer (for pyrophyllite and talc). Increases in precipitate stability were observed during Al-for-Ni and silicate-for-nitrate substitutions. Macroscopic dissolution studies showed an increase in Ni surface precipitate stability with aging. The aging effect was attributed partially to the solid-state transformation of the precipitate phases (silication of Ni–Al LDH and α-Ni hydroxide) and to crystal growth due to Ostwald ripening. Thompson *et al.* (15) established solubility constants for Co–Al LDH and found also that the Al-containing phase was less soluble than Co–hydroxide and Co–carbonate at circumneutral pH.

Accordingly, the objectives of this study were to examine the kinetics of the formation and dissolution of Ni surface precipitates in a gibbsite/amorphous silica mixture employing X-ray absorption fine structure (XAFS) spectroscopy, diffuse reflectance spectroscopy (DRS), and high-resolution thermogravimetric analysis (HRTGA). The sorption investigations observed the influence of aging on the α-Ni(OH)$_2$ precipitates and their subsequent conversion to a Ni–phyllosilicate precursor. The dissolution studies explored the effects of EDTA and HNO$_3$ in removing Ni from the precipitates.

2. MATERIALS AND METHODS

2.1. Materials

The mixture of gibbsite and amorphous silica consisted of 40% gibbsite and 60% silica by weight. A mixture was used to more closely mimic heterogeneous systems in the natural environment. The gibbsite (Arkansas, USA; Ward's) was derived from a natural deposit and was prepared by grinding the mineral in a ceramic ball mill for approximately 14 days, centrifuging to collect the <2-μm fraction in the supernatant, which was Na$^+$ saturated, and then removing excess salts by dialysis followed by freeze drying of the material. X-ray diffraction (XRD) showed minor impurities of about 10% bayerite in the gibbsite. The amorphous silica (SiO$_2$) (Zeofree 5112) was obtained from the

Huber Corp. The N$_2$ BET surface areas of the sorbent phases were 25 m^2 g^{-1} for gibbsite and 90 m^2 g^{-1} for amorphous silica. The mixture had an effective surface area of 64 m^2 g^{-1}.

The dissolution agents employed in the study were nitric acid (HNO$_3$) at pH 4 to induce proton-promoted dissolution and 1 mM ethylenediaminetetraacetic acid (EDTA) at pH 7.5 to induce ligand-promoted dissolution. EDTA forms a stable Ni solution complex, and previous studies have shown that EDTA promotes desorption of Ni sorbed to oxide surfaces and the dissolution of poorly crystalline oxide phases (16, 17).

2.2. Ni Sorption and Kinetics of Dissolution

To investigate the influence of aging on the stability of the precipitate phases, the gibbsite/silica mixture was reacted with Ni for periods of 1 day to 1 year. Experimental conditions were as described in Scheidegger and Sparks (2) using an initial concentration of 3 mM Ni as Ni(NO$_3$)$_2$, 10 g/L sorbents, and a background electrolyte of 0.1 M NaNO$_3$ at pH 7.5. The systems were purged with N$_2$ to eliminate CO$_2$, and the pH was maintained through addition of 0.1 M NaOH via a Radiometer pH-stat titrator. Periodic 10-ml aliquots were removed and centrifuged at 17,000 rpm for 5 min to obtain the supernatant for ICP analysis of Ni and Si during the sorption study. After 1 week, the batch reaction vessel was removed from the pH stat and placed in a 25°C incubation chamber. The pH was subsequently adjusted weekly.

Synthesis of reference compounds for comparison in the HRTGA studies was similar to the methods of Ford *et al.* (1). The synthetic references were mixed with a dry gibbsite/silica mixture sample at a 1 : 100 weight ratio prior to HRTGA analysis. Significant weight loss events for α-Ni(OH)$_2$ (NO$_3^-$ interlayer), Si-exchanged α-Ni(OH)$_2$ (partial silication of the interlayer), and Ni–phyllosilicate reference compounds when combined with the gibbsite/silica mixture occurred at approximately 332, 438, and 533°C, respectively.

Dissolution was carried out by a replenishment technique using 1 mM EDTA at pH 7.5 or HNO$_3$ at pH 4.0. From the aging Ni/mixture suspensions, 30 ml (corresponding to 300 mg of solid) was withdrawn. After centrifuging at 17,000 rpm for 5 minutes, the supernatant was decanted, and 30 ml of the dissolution agent was added to the remaining solids. The suspensions were then placed on a reciprocating shaker at 25°C for 24 h. The extraction steps were repeated either 10 times (=10 days) for short-term (aged <1 month) or 14 days for long-term (aged ≥1 month) Ni sorption samples. A disadvantage of the replenishment technique is that there will inevitably be some dissolved Ni entrained in the clay paste and one could argue that, in the EDTA dissolution studies, Ni–EDTA complexes could form on the surface. However, this accounts for a very small percentage of the overall Ni released. This is supported by the fact that the rate of dissociation for Ni–EDTA complexes is slow relative to the residence time of the complexes in solution before replenishment (18–20). The conditional stability constant (K^{cond}) for Ni–EDTA complexes is approximately 10^{10} M^{-1}. Sorption of Ni–EDTA complexes is also unlikely under the reaction

conditions of this study (21–24), suggesting the complexes prefer to remain in solution once formed. Additionally, the maximum solution concentration of Ni after any given 24-h replenishment period was 0.46 mM, which is far below the saturation point for re-precipitation of Ni under these reaction conditions either on the sorbent or in bulk solution, especially during dissolution with HNO_3 at pH 4.0. ICP-AES or AAS was used to determine Ni and Si in the supernatants during dissolution.

2.3. Spectroscopic and Thermogravimetric Characterization of Surface Precipitates

Changes in the solid-phase Ni speciation during sorption and dissolution were periodically assessed via spectroscopic and thermoanalytical techniques. For XAFS and DRS analyses, samples were examined *in situ* by centrifuging the suspensions and using the wet sorbent paste. For HRTGA analyses, the pastes were washed three times with D.I. water and freeze-dried before examination. Speciation of dissolution samples by HRTGA was carried out for samples aged for 1 month to ensure that only a negligible part of the Ni was bound as adsorbed mononuclear surface complexes and the majority as a precipitate. The 1-month aging time also allowed for repeated experiments in terms of available time.

XAFS was applied to determine information on the local chemical environment of sorbed Ni. Data acquisition was conducted at the National Synchrotron Light Source (NSLS), Brookhaven National Laboratory (BNL), Upton, New York, on beamline X-11A. The electron storage ring was operated at 2.528 GeV with beam currents in the 180- to 310-mA range. A 0.5-mm premonochromator slit width and a Si(111) double-crystal monochromator detuned by 25% to reject higher order harmonics was used. The beam energy was calibrated by assigning the first inflection of the $K\alpha$-absorption edge of nickel metal to 8333 eV. The XAFS spectra were collected in fluorescence mode using a Lytle detector. The ionization chamber of the Lytle detector was filled with Ar and the chamber of I_0 was filled with N_2 gas. Samples were positioned at a 45° angle relative to the incident beam and the ionization chamber was situated at 45° off the sample (90° off the incident beam). A Co-3 filter and Soller slits were arranged between the sample and the Lytle detector to reduce scattered X-rays reaching the fluorescence detector. Spectra were collected at 77 K to reduce thermal disorder. Previous studies in our laboratory indicate that Ni speciation does not change by cooling to 77 K versus room temperature (13). Triplicate scans were collected for each sample.

MacXAFS 4.0 (25) was employed for background subtraction and Fourier filtering. The χ function was extracted from the raw data by using a linear pre-edge background and a spline postedge background and by normalizing the edge to unity. The data were next converted from energy to k space and weighted by k^3 to compensate for the dampening of the XAFS amplitude with increasing k. Structural parameters were extracted with fits to the standard XAFS equation. Using the FEFF6 and ATOMS codes (26), *ab initio* amplitude and phase functions for single shells

were calculated. A synthetic β-Ni(OH)$_2$ (Johnson Mattey Co.) was used as a reference compound. Multishell fitting was done in R space over the range $1.104 < R < 3.191$ Å with $3.2 < k < 13.6$ Å^{-1} for the mixture sorption samples. The number of free floating parameters was reduced by one by allowing only equal values for the Debye–Waller factors of the Ni–Ni and Ni–Si shells for the 6-month and 1-year aged samples. The R_{Ni-O} and R_{Ni-Ni} values are estimated to be accurate to ±0.02 Å, and the N_{Ni-O} and N_{Ni-Ni} values are estimated to be accurate to ±20%. The estimated accuracies for N_{Ni-Si} and R_{Ni-Si} are ±60% and ±0.06 Å, respectively. The accuracy estimates are based on the results of theoretical fits to spectra of the reference compounds of known structure (27).

Although the information provided by DRS is restricted to local symmetry of the first coordination shell, it is more sensitive to changes in the coordination distance of Ni–O (R_{Ni-O}) than XAFS. It has been shown that this method is very sensitive in distinguishing between Ni–Al LDH (smaller R_{Ni-O}) and α-Ni hydroxide (larger R_{Ni-O}) by using the energy position of the $\nu2$ band, which corresponds to the $^3A_{2g} \rightarrow {}^3T_{1g}$ transition (9). A Perkin–Elmer Lambda 9 diffuse reflectance spectrophotometer fitted with a 5-cm Spectralon-coated integrating sphere was employed to collect spectra in the UV–vis–NIR range. Extraction of the band position was as that in Scheinost *et al.* (9).

HRTGA was employed to characterize thermal decomposition reactions attributed to the Ni precipitate phases in the reacted mixture samples. Changes in the quantity and temperature of decomposition are indicative of compositional changes in the precipitate. We employed a TA Instruments 2950 high-resolution thermogravimetric analyzer to examine approximately 15- to 20-mg samples from sorption and dissolution studies that were previously freeze-dried. The analysis was conducted under a N_2 atmosphere over a temperature range of 30–600°C. The following high-resolution settings were used: (1) maximum heating rate = 20°C min^{-1}, (2) resolution = 5.0, and (3) sensitivity = 1.0 (28). Data are presented as the derivative of the weight loss curve versus temperature with the derivative weight loss curve for an unreacted gibbsite/silica mixture sample subtracted out so that only weight loss events associated with the Ni precipitates are observed.

3. RESULTS AND DISCUSSION

3.1. Sorption Data

The kinetics of Ni sorption and Si release in the gibbsite/silica mixture are shown in Fig. 1. An initial rapid uptake of Ni occurred in which over 90% of the Ni was sorbed within 72 h was followed by a slow sorption period. Release of Si from the sorbent during sorption mimics the removal curve of Ni from solution. This behavior suggests that Ni may be influencing the release of Si during the sorption process and has been noted as metal-promoted dissolution (7). The released Si is subsequently available for incorporation into the Ni precipitate interlayer to replace nitrate.
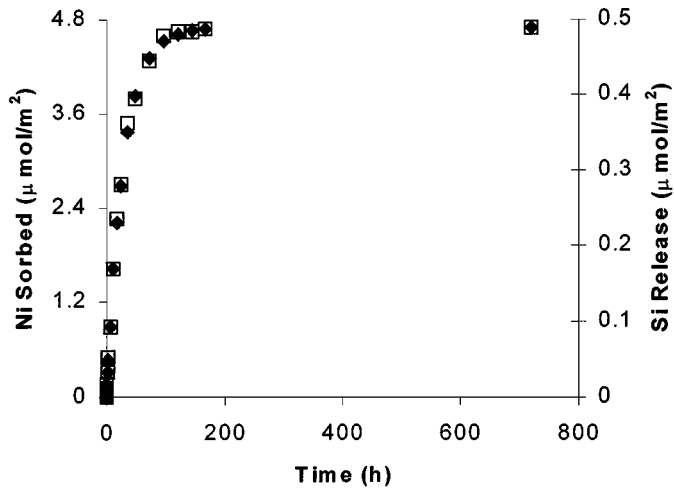
FIG. 1. Ni sorption and Si release kinetics on a gibbsite/amorphous silica mixture at pH 7.5, $I = 0.1$ M $NaNO_3$, $[Ni]_0 = 3$ mM, and solid : solution = 10 g/L.

The k^3-weighted, normalized, background-substracted, Fourier-transformed radial structure functions (RSF) (solid lines) for Ni sorbed on the mixture and theoretical spectra (dotted lines) derived by fitting Ni–O, Ni–Ni, and Ni–Si scattering

paths to the raw data are presented in Fig. 2. The spectra are uncorrected for phase shift. The excellent correlation between the raw data and theoretical fits indicate a good representation of the experimental data. The structural parameters obtained from the fits are listed in Table 1. Analysis shows that the first shell is consistent with Ni coordinated to 6 O atoms, indicating that Ni is in an octahedral coordination environment. The Ni–O bond distance (R_{Ni-O}) is approximately 2.05 Å in all samples with a constant coordination number (N_{Ni-O}) of 6. The data fit for the second shell indicates the presence of a second neighbor Ni atom at an average bond (R_{Ni-Ni}) distance of 3.08 Å and a coordination (N_{Ni-Ni}) of approximately 6 Ni atoms. As the reaction time increased from 1 h to 7 days, the amount of Ni on the mixture surface increased, leading to a more pronounced second shell as the reaction time progressed. To improve the fit, Si was included in fitting the second shell for the 6-months and 1-year aged samples to yield a Ni–Si bond distance (R_{Ni-Si}) of ~3.28 Å and a fixed coordination number (N_{Ni-Si}) of 2, suggesting the formation of a Ni phyllosilicate at these later aging times.

Based on previous studies by Scheinost *et al.* (9) and Scheinost and Sparks (11), a Ni–Ni bond distance of 3.08 Å is consistent with the formation of α-Ni(OH)$_2$ precipitates. To further confirm the identify of the precipitates formed on the mixture, we compared the χ functions of 1-month aged precipitates on
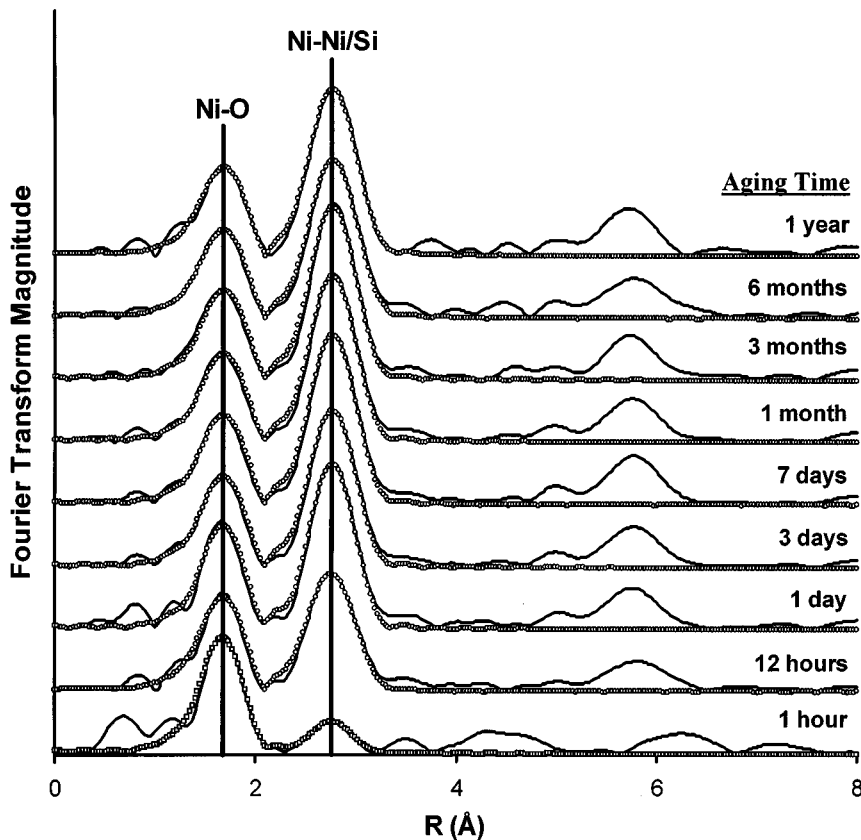

FIG. 2. Ni $K\alpha$ XAFS spectra of the measured (solid lines) and fitted (dotted lines) radial structure functions (uncorrected for phase shifts) of a gibbsite/amorphous silica mixture reacted with Ni for various aging times.

TABLE 1
XAFS Structural Parameters for Ni Sorption in a Gibbsite/Silica Mixture

Aging time	ΔE_0	Ni–O			Ni–Ni			Ni–Si		
		R (Å)[a]	N[b]	σ^2 (Å²)[c]	R (Å)[a]	N[b]	σ^2 (Å²)[c]	R (Å)[a]	N[b]	σ^2 (Å²)[c]
1 year	0.5	2.06	6.0	0.004	3.08	6.2	0.004	3.28	2.0	0.004
6 months	0.5	2.05	6.0	0.004	3.09	6.2	0.004	3.28	2.0	0.004
3 months	0.3	2.06	6.0	0.004	3.08	6.6	0.004			
1 month	0.1	2.05	6.0	0.004	3.08	6.9	0.004			
7 days	0.1	2.05	6.0	0.004	3.08	6.9	0.003			
3 days	0.2	2.05	6.0	0.003	3.08	6.5	0.003			
1 day	0.6	2.05	6.0	0.003	3.08	5.7	0.003			
12 h	0.8	2.05	6.0	0.004	3.08	5.3	0.004			
1 h	1.6	2.05	6.0	0.003	3.08	0.8	0.001			

[a] Interatomic distance.
[b] Coordination number.
[c] Debye–Waller factor.

silica, gibbsite, and the gibbsite/silica mixture (Fig. 3). Scheinost *et al.* (9) and Scheinost and Sparks (11) demonstrated that α-Ni(OH)$_2$ precipitates form on silica and mixed Ni–Al LDH phases form on gibbsite with bond distances of 3.08 and 3.06 Å, respectively. The structural difference between these two phases is that the LDH phase has Al substituted into the Ni octahedral sheets and this induces a distinctly shorter Ni–Ni bond of 3.06 Å. Additionally, there is a characteristic beat pattern (indicated with the circles in Fig. 3) at approximately 8 Å^{-1} that is dampened when Ni–Al LDH precipitates are present. One can see that indeed the peak at 8 Å^{-1} is dampened for the precipitates associated with gibbsite; however, this reduction in oscillation is not apparent in the silica and mixture curves, confirming that α-Ni(OH)$_2$ precipitates are forming on the gibbsite/silica mixture. These results are somewhat contradictory from previous

FIG. 3. The k^3 weighted χ functions of 1-month-aged Ni-reacted silica, gibbsite, and gibbsite/silica mixture samples. Listed to the right are the Ni–Ni bond distances (R_{Ni-Ni}) derived from theoretical fits of EXAFS data and the corresponding precipitate phase that results. The circles show key identification for Ni–Al LDH versus α-Ni hydroxide (9).

studies that assume that since an Al source is present in solution (i.e., with gibbsite), Ni–Al LDH phases should form. However, studies that have examined Ni sorption on gibbsite (8–11) noted that the precipitation kinetics were relatively slow. Additionally, Al release from gibbsite at pH 7.5 is very gradual due to the low solubility of gibbsite (log $K_{SO} = 9.61$); therefore, available Al for the formation of Ni–Al LDH precipitates is small given the rapid sorption kinetics seen for the gibbsite/silica mixture. Therefore, the silica phase of the mixture appears to be dominating the sorption kinetics, which explains the formation of α-Ni(OH)$_2$ precipitates.

The crystal field splitting of Ni^{2+} in an octahedral O cage is very sensitive to small changes in Ni–O bond distances (29). Therefore, DRS can be used to distinguish between Ni–Al LDH, Ni phyllosilicate, and α-Ni hydroxide (9). Consistent with the XAFS results shown before, the $\nu 2$ band position of 14,800 cm^{-1} for the gibbsite/silica mixture (Fig. 4a) indicates α-Ni hydroxide and the $\nu 2$ band position of 15,060 cm^{-1} for the mixture at longer aging times indicates the formation of a Ni–phyllosilicate precursor. Because the absorption coefficient of aqueous Ni^{2+} complexes is 2 orders of magnitude lower than that of Ni^{2+} in a three-dimensional, polynuclear structure, band heights are indicative of the amount of Ni present in a precipitate phase (9). Therefore, at the earlier reaction times of 1–7 days (Fig. 4b), a continuum between adsorption and precipitation may be occurring, explaining the smaller peak sizes, and is supported in the growth of the second shell for the XAFS analysis (Fig. 2).

Our high-resolution thermogravimetric analysis (HRTGA) results indicate that the initially formed α-Ni(OH)$_2$ precipitates in the gibbsite/silica mixture transforms into a Ni phyllosilicate precursor within 1 year at ambient reaction conditions. The derivatives of the HRTGA weight loss curves (Fig. 5) show weight loss events associated with the gibbsite, silica, and mixtures of the surfaces unreacted with Ni. One can see that the curve for the mixture is a combination of both gibbsite and silica curves. Since there is a major weight loss occurrence at about
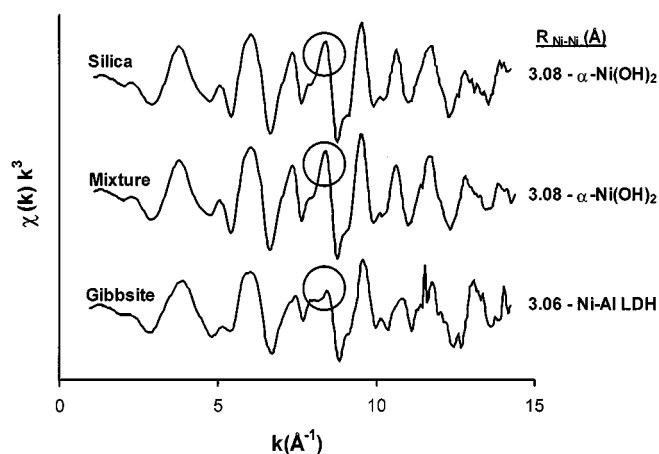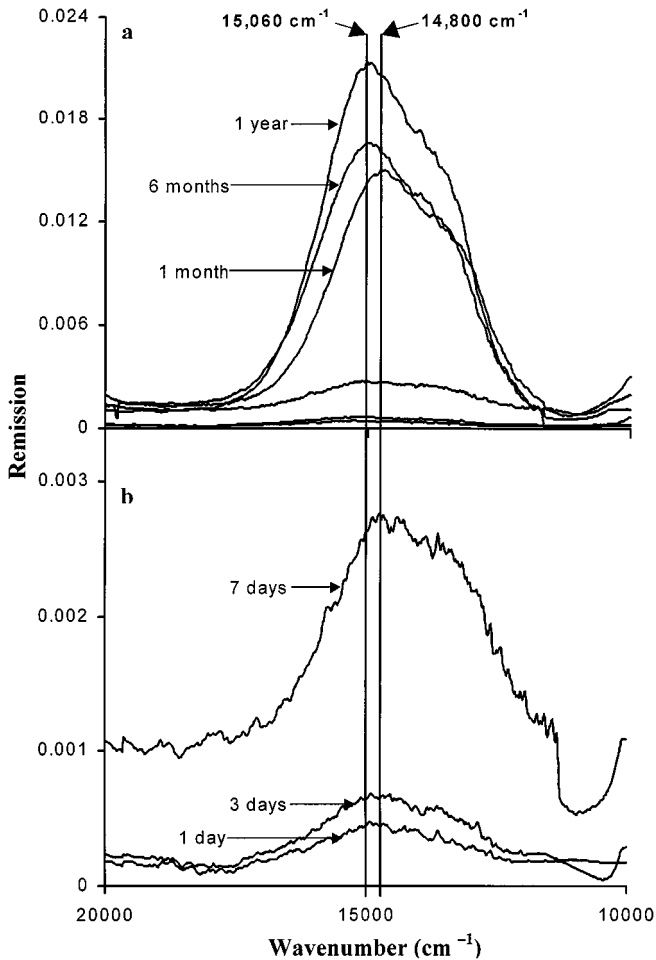
FIG. 4. The DRS $\nu2$ bands for the Ni surface precipitates on the gibbsite/amorphous silica mixture for various aging times. (a) All spectra collected; note that the three smaller curves for the early reaction times are unmarked. (b) Spectra were collected for reaction times of 1–7 days with an expanded y axis.
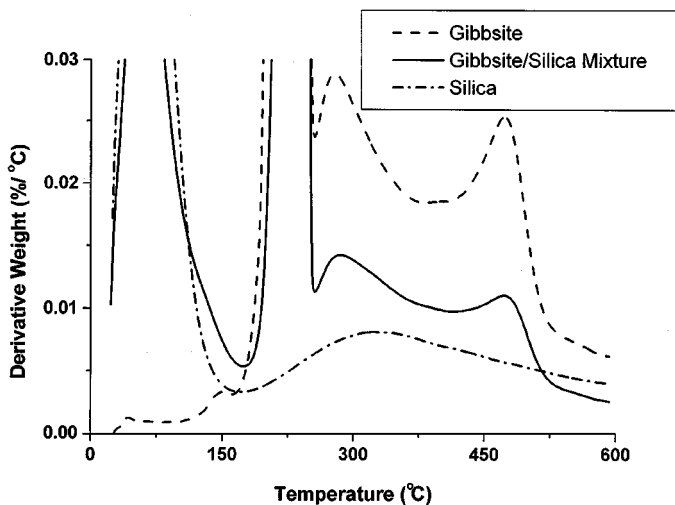

FIG. 5. The derivative of the weight loss curves for gibbsite, silica, and the gibbsite/silica mixture unreacted with Ni.
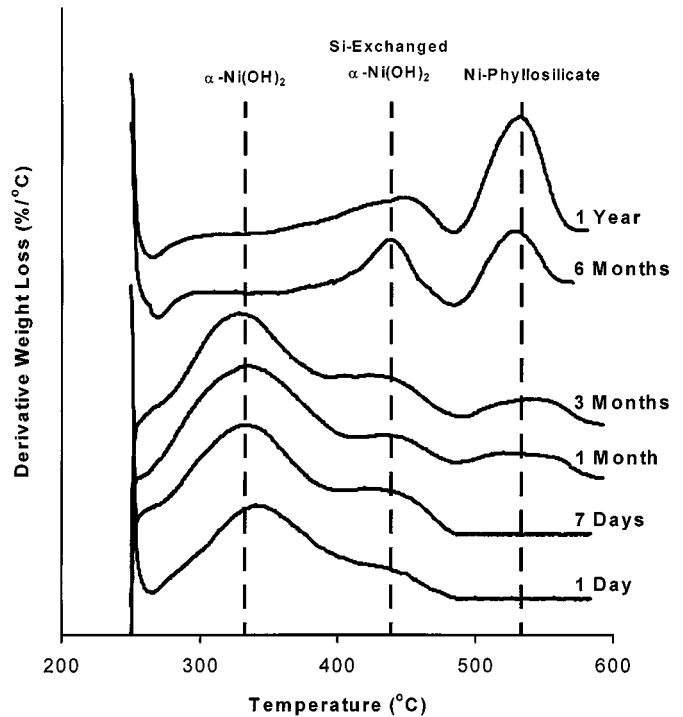

FIG. 6. Changes in the thermal stability of the Ni surface precipitates on the mixture showing the conversion from α-Ni(OH)$_2$ to a Ni phyllosilicate with aging. The derivative weight loss curves are background subtracted from an unreacted sample (Fig. 5) to show only weight loss events associated with the precipitate phases. The identification markers are derived from reference compounds.

230°C for the gibbsite surface, no weight loss at 220°C is detectable, which would occur due to water and nitrate expulsion for the interlayer (1, 31). To observe only weight loss events associated with the Ni precipitates on the mixture, we subtracted the curve for the unreacted mixture surface from the curves for the sorption samples (Fig. 6). One sees for the 1- and 7-day samples a substantial α-Ni(OH)$_2$ peak with a small shoulder in the Si-exchanged interlayer α-Ni(OH)$_2$ region and no indication of Ni phyllosilicate. The 1- and 3-month curves show evidence of α-Ni(OH)$_2$ and Si-exchanged α-Ni(OH)$_2$ precipitates with a small peak arising at the Ni phyllosilicate marker. For the long-term aging times of 6 months and 1 year, one notices very little α-Ni(OH)$_2$ but well-defined peaks comparable with the Si-exchanged α-Ni(OH)$_2$ and Ni phyllosilicate reference precipitates. The data from the HRTGA experiments demonstrate that Ni sorption on the gibbsite/silica mixture results initially in the formation of α-Ni(OH)$_2$ precipitates followed by Si-exchanged α-Ni(OH)$_2$ and with time the subsequent conversion to a Ni phyllosilicate. This transformation progresses by silicate-for-nitrate exchange in the interlayer, and the subsequent polymerization of single silicate units, which may then become connected with the octahedral hydroxide layers (30). This transformation leads to increasingly stable surface precipitates that will be addressed further in the dissolution results section.

3.2. Dissolution Data

The macroscopic dissolution data are assembled in Fig. 7 and are presented as the relative amount of Ni remaining on the surfaces. For both dissolution agents, the fraction of extracted Ni generally decreased as the age of the Ni complexes increased from 1 day to 1 year. As expected, the ligand-promoted dissolution by EDTA (Fig. 7a) is more effective than the protolysis by HNO_3 (Fig. 7b) (17). After 1 month and 1 year of aging, less than 17% and 4% of the sorbed Ni is released by HNO_3 after 14 days of dissolution, respectively. Aging also decreases Ni release by EDTA as seen by 65% and 93% of the sorbed Ni remaining on the mixture after 1 month and 1 year of residence time for 14 replenishment treatments. The differences in the amount of Ni removed from the mixture for 1-month and 1-year aging times further supports the transformation of the precipitate phase to a more stable phyllosilicate precursor, as seen in the HRTGA results (Fig. 6).

An important point to consider during these dissolution experiments is the stability of the sorbent surface. In addition to analyzing for Ni in the dissolution studies, Si was also quanti-
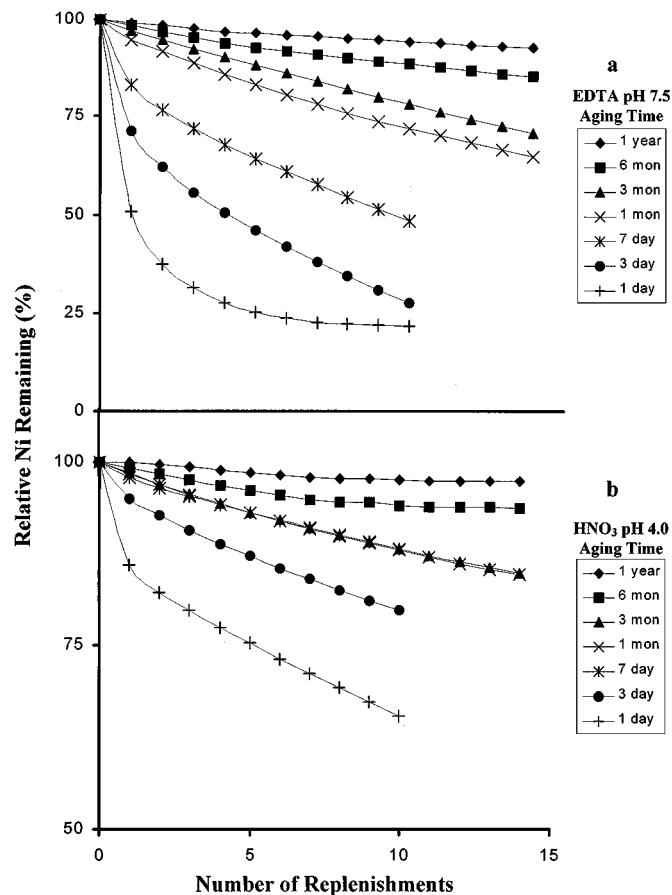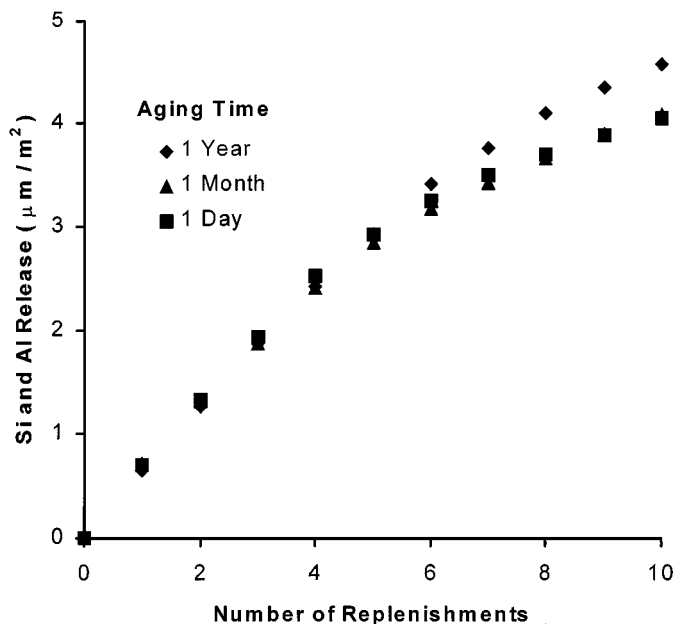

FIG. 8. Release of Si during dissolution of 1-day, 1-month, and 1-year-aged Ni mixture samples employing 1 mM EDTA at pH 7.5.

fied. Si release during dissolution was comparable regardless of the aging time of the precipitates. Figure 8 shows total Si dissolution with EDTA (pH 7.5) from the sorbent and precipitate for sorption aging times of 1 day, 1 month, and 1 year. What we believe to be transpiring during the dissolution process is a congruent dissolving of the Ni precipitate in addition to the sorbent surface. This makes it difficult to distinguish Si release from the interlayer of the Ni precipitates and the surface except at early reaction times when very little Si has exchanged into the interlayer. Although not shown, a similar Si release trend was observed during dissolution with nitric acid (pH 4.0).

Earlier, HRTGA was employed to show that α-Ni(OH)$_2$ precipitates on the gibbsite/silica mixture transform into a Ni phyllosilicate precursor within 1 year under ambient reaction conditions. We also used HRTGA to examine the dissolution of the Ni precipitates aged for 1 month on the mixture utilizing HNO_3 at pH 4.0 (Fig. 9). The curve for the mixture unreacted with Ni was subtracted from these curves to view only weight loss events associated with the Ni precipitates. The untreated curve represents a 1-month-aged Ni mixture sample prior to dissolution. The other curves are the result of dissolution with nitric acid for 1, 7, and 14 days or replenishment treatments. The amount of Ni remaining on the mixture surface is noted in the figure legend and as one can see only 15% of the Ni is released from the surface over the reaction period. The size of each peak is indicative of the amount of each particular phase present on the surface. Decreases in the size of the peaks associated with α-Ni(OH)$_2$ are more pronounced than those in conjunction with the Si-exchanged α-Ni(OH)$_2$ precipitates, and only minor changes are observed for the peak, indicating the presence of Ni phyllosilicate. These results are in line with recent
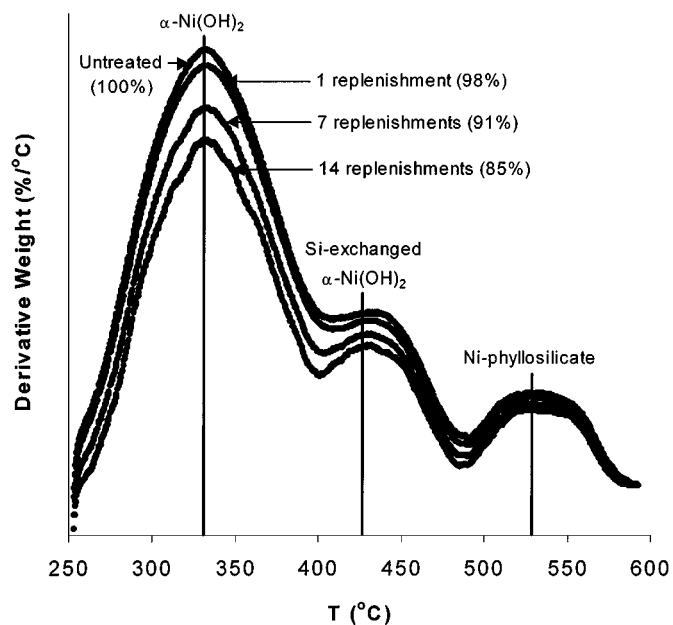

FIG. 7. Macroscopic dissolution behavior of aged Ni precipitates on a gibbsite/amorphous silica mixture showing the relative amount of Ni remaining on the mixture surface following extraction with (a) 1 mM EDTA at pH 7.5 and (b) HNO_3 at pH 4.0 plotted against the total number of replenishments. The stability of the Ni precipitates increases with aging time.

FIG. 9. Background subtracted HRTGA of Ni surface precipitates on the gibbsite/amorphous silica mixture aged for 1 month ("untreated") and following 1, 7, and 14 replenishment dissolution steps with HNO_3 (pH 4). The relative percentages of Ni remaining on the surface are noted in the parentheses. The weight loss events at about 332, 438, and 533°C are indicative of α-Ni(OH)$_2$, Si-exchanged α-Ni(OH)$_2$, and Ni phyllosilicate.

work by Scheckel *et al.* (14) that examined dissolution of synthetic α-Ni(OH)$_2$ and Si-exchanged α-Ni(OH)$_2$ precipitates in which the silicated phase was more resistant to dissolution. One could easily hypothesize that the Ni phyllosilicate is even more resistant to dissolution than α-Ni(OH)$_2$ and Si-exchanged α-Ni(OH)$_2$. Although not shown, similar results were observed during dissolution of 1-month-aged Ni mixture samples with EDTA at pH 7.5.

4. SUMMARY

In this study, we examined the kinetics and mechanisms of the formation and the dissolution of Ni precipitates on a gibbsite/amorphous silica mixture using advanced analytical and spectroscopic techniques. We provided evidence using HRTGA, XAFS, and DRS for the solid-state transformation of an initial α-Ni(OH)$_2$ precipitate to a Ni phyllosilicate with time in our sorption experiments. This process was driven by the release of Si from the sorbent mixture during Ni sorption, thus allowing the available Si to substitute into the interlayer for nitrate and lead to further conversion into a phyllosilicate precursor.

The macroscopic dissolution studies demonstrated increased stability in Ni surface precipitates with aging as seen by less release of Ni from the surface. EDTA was more effective in removing Ni from the precipitates than HNO_3, particularly at earlier aging times. The aging effect may be attributed to the solid-state transformation of the precipitate phases through silication of the interlayer. HRTGA results indicated that, with dissolu-

tion time, less stable phases dissolved at a slightly greater rate (α-Ni(OH)$_2$ > Si-exchanged α-Ni(OH)$_2$ > Ni phyllosilicate).

REFERENCES

1. Ford, R. G., Scheinost, A. C., Scheckel, K. G., and Sparks, D. L., *Environ. Sci. Technol.* **33**(18), 3140–3144 (1999).
2. Scheidegger, A. M., and Sparks, D. L., *Chem. Geol.* **132,** 157–164 (1996).
3. Towle, S. N., Bargar, J. R., Brown, G. E., Jr., and Parks, G. A., *J. Colloid Interface Sci.* **187,** 62–82 (1997).
4. Thompson, H. A., Parks, G. A., and Brown, G. E., Jr., *Geochim. Cosmochim. Acta* **63,** 1767–1779 (1999).
5. d'Espinose de la Caillerie, J. B., Kermarec, M., and Clause, O., *J. Am. Chem. Soc.* **117,** 11471–11481 (1995).
6. Scheidegger, A. M., Fendorf, M., and Sparks, D. L., *Soil Sci. Soc. Am. J.* **60,** 1763–1772 (1996).
7. Scheidegger, A. M., Lamble, G. M., and Sparks, D. L., *J. Colloid Interface Sci.* **186,** 118–128 (1997).
8. Scheidegger, A. M., Strawn, D. G., Lamble, G. M., and Sparks, D. L., *Geochim. Cosmochim. Acta* **62,** 2233–2245 (1998).
9. Scheinost, A. C., Ford, R. G., and Sparks, D. L., *Geochim. Cosmochim. Acta* **63,** 3193–3203 (1999).
10. O'Day, P. A., Brown, G. E., Jr., and Parks, G. A., *J. Colloid Interface Sci.* **165,** 269–289 (1994).
11. Scheinost, A. C., and Sparks, D. L., *J. Colloid Interface Sci.* **223,** 167–178 (2000).
12. Elzinga, E. J., and Sparks, D. L., *J. Colloid Interface Sci.* **213,** 506–512 (1999).
13. Roberts, D. R., Scheidegger, A. M., and Sparks, D. L., *Environ. Sci. Technol.* **33**(18), 3749–3754 (1999).
14. Scheckel, K. G., Scheinost, A. C., Ford, R. G., and Sparks, D. L., *Geochim. Cosmochim. Acta* in press (2000).
15. Thompson, H. A., Parks, G. A., and Brown, G. E., Jr., *Clays Clay Miner.* **47,** 425–438 (1999).
16. Borggaard, O. K., *Z. Pflanzeñernähr. Bodenk.* **155,** 431–436 (1992).
17. Bryce, A. L., and Clark, S. B., *Colloids Surf.* **107,** 123–130 (1996).
18. van den Berg, C. M. G., and Nimmo, M., *Sci. Total Environ.* **60,** 185–195 (1987).
19. Hering, J. G., and Morel, F. M. M., *Environ. Sci. Technol.* **24,** 242–252 (1990).
20. Wilkins, R., "The Study of Kinetics and Mechanisms of Reactions of Transition Metal Complexes." Allyn & Bacon, Boston, MA, 1974.
21. Elliott, H. A., and Huang, C. P., *J. Colloid Interface Sci.* **70,** 29–44 (1979).
22. Elliott, H. A., and Denney, C. M., *J. Environ. Qual.* **11,** 658–663 (1982).
23. Chang, C., and Ku, Y., *J. Hazard. Mater.* **38,** 439–451 (1994).
24. Nowack, B., and Sigg, L. J., *J. Colloid Interface Sci.* **177,** 106–121 (1996).
25. Bouldin, C., Elam, T., and Furenlid, L., *Physica B* **208/209,** 190–192 (1995).
26. Zabinsky, S. I., Rehr, J. J., Ankudinov, A., Albers, R. C., and Eller, M. J., *Phys. Rev. B* **52,** 2995 (1995).
27. O'Day, P. A., Rehr, J. J., Zabinsky, S. I., and Brown, G. E., Jr., *J. Am. Chem. Soc.* **116,** 2938–2949 (1994).
28. Ford, R. G., and Bertsch, P. M., *Clays Clay Miner.* **47**(3), 329–337 (1999).
29. Burns, R. G., "Mineralogical Applications of Crystal Field Theory." Cambridge Univ. Press, Cambridge, U.K., 1993.
30. Depège, C., El Metoui, F.-Z., Forano, C., de Roy, A., Dupuis, J., and Besse, J.-P., *Chem. Mater.* **8,** 952–960 (1996).
31. Bellotto, M., Rebours, B., Clause, O., Lynch, J., Bazin, D., and Elkaim, E., *J. Phys. Chem.* **100,** 8535–8542 (1996).